Characterizing the Charge Trapping across Crystalline and Amorphous $Si/SiO_2/HfO_2$ Stacks from First-Principle Calculations

Yue-Yang Liu,[1,2] Feilong Liu,[1] Runsheng Wang,[3,*] Jun-Wei Luo,[1,†] Xiangwei Jiang,[1,‡] Ru Huang,[3] Shu-Shen Li,[1] and Lin-Wang Wang[2,§]

[1] *State Key Laboratory of Superlattices and Microstructures, Institute of Semiconductors, Chinese Academy of Sciences, Beijing 100083, China*

[2] *Joint Center for Artificial Photosynthesis and Materials Science Division, Lawrence Berkeley National Laboratory, Berkeley, California 94720, USA*

[3] *Institute of Microelectronics, Peking University, Beijing 100871, China*

(Received 28 April 2019; revised manuscript received 22 October 2019; published 5 December 2019)

The complexity of charge trapping in semiconductor devices, such as high-κ MOSFETs, is increasing as the devices themselves become more complicated. To facilitate research into such charge-trapping issues, here we propose an optimized simulation framework that is composed of density-functional theory (DFT) for electronic structure calculation and Marcus theory for the calculation of charge-trapping rates. The DFT simulations are either carried out or corrected by using the Heyd-Scuseria-Ernzerhof hybrid functional. Using this framework, the hole-trapping characteristics along multiple paths in $Si/SiO_2/HfO_2$ stacks are investigated, and the relative importance of each path is revealed by calculating its exact hole-trapping rate. Besides the study on crystalline stacks, we also create an amorphous stack, which is more realistic compared with experiments and real devices, to reveal more active trapping centers and to study the statistical feature of charge trapping induced by structural disorder. In addition, to seek effective measures for relieving these charge-trapping problems, the effects of hydrogen and fluorine passivations are discussed, and physical insights for improving the performance of high-κ MOSFETs are provided.

DOI: 10.1103/PhysRevApplied.12.064012

I. INTRODUCTION

Charge trapping from semiconductors to the coated oxide/nitride/high-κ layers is a very important quantum mechanical process in semiconductor physics and applications. On one hand, charge trapping can be utilized to store information in semiconductor-oxide-nitride-oxide-semiconductor (SONOS) capacitor structures to form nonvolatile memory devices [1,2]. On the other hand, charge trapping is a severe problem that needs to be solved to improve the reliability of MOSFETs [3,4], especially high-κ MOSFETs, which replace conventional SiO_2/SiO_xN_y gate dielectrics with high-κ materials to reduce gate leakage currents during continuous size scaling [5–7]. Desirable in one case and problematic in the other case, charge trapping is definitely a key physical process that must be well understood in order to control it in different situations. However, in both cases, as shown schematically in Fig. 1, the charge-trapping process can occur across multiple interfaces, such as Si/SiO_2, SiO_2/Si_3N_4, and SiO_2/HfO_2 interfaces, which makes the physics complicated and difficult to comprehend, especially if one tries to find out the results merely from fitting to experimental device performance. It will thus be very useful if the problem can be studied by first-principle calculations, and different cases can be classified according to their distinct physical behaviors.

The charge-trapping phenomenon in MOSFETs is a general process, in which carriers in the semiconductor channel are transferred into the gate dielectrics by crossing single or multiple interfaces, and finally trapped in the defective or intrinsic trapping centers in the dielectric oxides. Static defect properties related to the charge-trapping process have been investigated widely by using first-principles calculations, e.g., the trap energy levels, wave functions, and formation or transition energies. [8–14]. However, studies on the entire charge-trapping process, including the whole heterostructure and related charge-transfer dynamics, all at the *ab initio* level are much scarcer. One possible reason for such a situation is that the charge-trapping phenomenon in MOSFETs had not been paid sufficient attention until Grasser *et al.* emphasized its importance on the bias temperature instability (BTI)

*r.wang@pku.edu.cn
†jwluo@semi.ac.cn
‡xwjiang@semi.ac.cn
§lwwang@lbl.gov

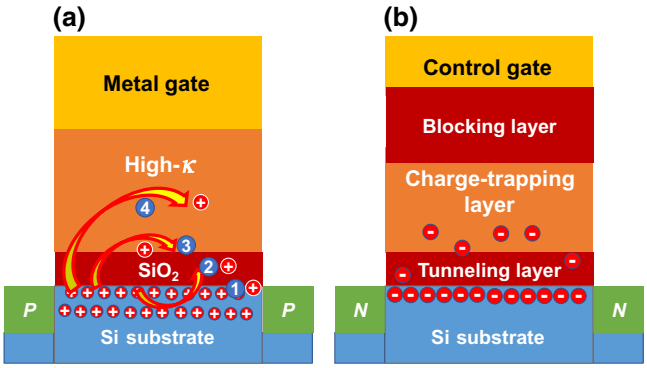

FIG. 1. Schematic of high-κ MOSFETs (a) and charge-trapping-based nonvolatile memory cells (b). The multiple charge-trapping paths are marked.

[4,15–17]. Another reason is that such simulations on the whole heterostructures are often beyond the capability of previous *ab initio* calculations methods and codes, and there are also other technical issues, ranging from interface and amorphous structures to how to calculate the charge-transfer rates.

As discussed in one of our previous studies on charge trapping across Si/SiO_2 interfaces [18], accurate atomistic simulation of the charge-trapping process is possible only after a few technical challenges are overcome. These include realistic interface structures, correct theoretical band alignment, and the application of adequate charge-transfer theories. Undoubtedly, the existence of multiple interfaces will make the calculation even more challenging. First, the construction of atomistic models with multiple interfaces is difficult due to lattice mismatch of different materials. Second, the computational cost can be very high because a system with multiple interfaces is usually very large. Third, an increase in material types and interface numbers will greatly enhance the amount of possible defect candidates, including defects in each material and defects at each interface. A systematic study taking into account all of the above factors will be challenging. On the other hand, since the parameters needed to carry out a charge-transfer calculation, e.g., the electron-electron coupling, the reorganization energy, and the WKB decay length, are much less well known in multijunction cases than that in simple interface cases; this calls for the development of a first-principle calculation paradigm to solve this problem.

Here, we combine the methods we have developed before into an optimized simulation framework, which is able to simulate the charge-trapping process in most multiple interface systems, and then we apply it to the $Si/SiO_2/HfO_2$ gate stacks to investigate the hole-trapping process along different paths in high-κ gate transistors.

For charge trapping in HfO_2 dielectrics, it is demonstrated that oxygen vacancies (V_Os) should be the main charge traps because of their lower formation energies and closer energy levels with that of the Si band edge [19,20]. While such a conclusion is intuitively reasoned, it lacks a rigorous verification through quantitative calculations. Charge trapping from Si to HfO_2 in real high-κ gate transistors is much more complicated. First, the high-κ gate transistors always contain a thin SiO_2 interlayer between Si and HfO_2, so that the interface quality can be improved. Consequently, the energy level of oxygen vacancies in the $Si/SiO_2/HfO_2$ stacks will vary significantly, depending on their locations, e.g., at the SiO_2 layer, at the SiO_2/HfO_2 interface, or at the HfO_2 layer, instead of being a constant [21]. Experiments show that there are different defect levels in HfO_2 gate stacks [22,23]. It has also been reported that double V_Os could contribute more than a single V_O to random charging-discharging in HfO_2 [24]. Second, the energy barrier between the defect level and the Si band edge is not the only factor that determines the charge-trapping rate. The coupling strength between the two states also plays an important role [17,25]. It is proven that the coupling strength is especially important when the initial state and final state are close in energy [18]. Third, the energy level of the charge-trapping defect in the dielectric layer depends greatly on the applied gate voltage and so does the energy difference between these defect levels and the Si band edge. Finally, the hydrogen (H) or fluorine (F) passivation of the oxygen vacancy must be carefully considered because gas annealing is an indispensable process in transistor manufacture.

The framework proposed here will take all important factors of the charge-trapping process into consideration, including atomistic interfaces, trapping energy barriers, coupling strength, electron-phonon interactions, oxide electric fields, and H or F passivation. With this framework, we present the distinct hole-trapping characteristics along different paths in the $Si/SiO_2/HfO_2$ stacks and then reveal the mechanistic details of the charge-trapping process, including which quantity controls the trapping rate most, what role the multiple interfaces and various passivation processes play, and where the dominant traps are located under different magnitudes of electric field. Different from our previous work reported at a conference [26], here we spend additional efforts on studying the Si/SiO_2 interface defects and the effect of H and F passivation on all V_O defects at the Si/SiO_2 interface, SiO_2 bulk, the SiO_2/HfO_2 interface, and HfO_2 bulk. We also create an amorphous $Si/SiO_2/HfO_2$ interface stack, which is more realistic compared with that of experiments and actual microelectronic devices to investigate the influence of structural disorder. This information is of great concern for industrial engineers and has not been studied systematically. We also provide more details on Marcus theory and density-functional theory (DFT) calculations with respect to our systems. These theories and results will deepen our understanding of charge trapping in high-κ MOSFETs, and

thus, facilitate the solution of charge-trapping problems in high-κ MOSFETs and improve the integration of high-κ materials in silicon CMOS technology.

II. THEORY AND SIMULATION

A. Marcus charge-transfer theory

The charge-trapping probability is determined by multiple factors, including the energy barrier between the initial and final states, the electronic coupling strength between the two states, and electron-phonon interactions. A well-recognized formula to describe such a state-to-state charge-transfer rate is that proposed by Marcus in the 1950s [27,28], which is able to take all the factors mentioned above into consideration:

$$\nu = \frac{2\pi}{\hbar}|V_C|^2\sqrt{\frac{1}{4\pi\lambda k_B T}}\exp\left[-\frac{(\Delta G+\lambda)^2}{4\lambda k_B T}\right], \quad (1)$$

where V_C is the coupling constant between the initial and final states, ΔG is the total Gibbs free energy change for the charge-transfer reaction, and λ is the reorganization energy that stems from structural relaxation caused by charge trapping. It represents the strength of electron-phonon coupling. This Marcus formula has been successfully applied to semiconductor-molecule systems to study the electron- and hole-transfer dynamics [25,29,30].

A schematic description of Marcus theory and the charge-trapping process is shown in Fig. 2, in which the horizontal axis represents the structural configuration and the vertical axis is the energy of different configurations. According to the relative magnitudes of G_f and G_i, and the relative magnitudes of ΔG and λ, the energy diagram of Marcus charge-transfer theory can be divided into different situations. The four schematics shown in Fig. 2 represents the charge-trapping process from Si to SiO_2, SiO_2/HfO_2 interface and HfO_2 respectively, and all of them are results by the DFT calculations conducted in this work, which will be shown later. For the following conceptual discussion, any one of the four schematics can be used as the reference. At the beginning of the hole-trapping process, a hole lies on the valence band maximum of Si (E_{VBM}), and the energy of the system can be written as

$$G_i = E_0 - E_{\mathrm{VBM}} - \lambda_{\mathrm{Si}}, \quad (2)$$

where E_0 is total energy of the charge-neutral system and λ_{Si} is the reorganization energy caused by structural relaxation when the E_{VBM} is occupied by the hole. Then the hole transfers to the defect by crossing the energy barrier between E_{VBM} and the defect level (E_{defect}). Such a transition is induced by the coupling constant (V_C) between E_{VBM} and E_{defect}. After hopping, the atomic positions will experience a structural relaxation due to the occupation of the defect level by a hole, and the final energy of the

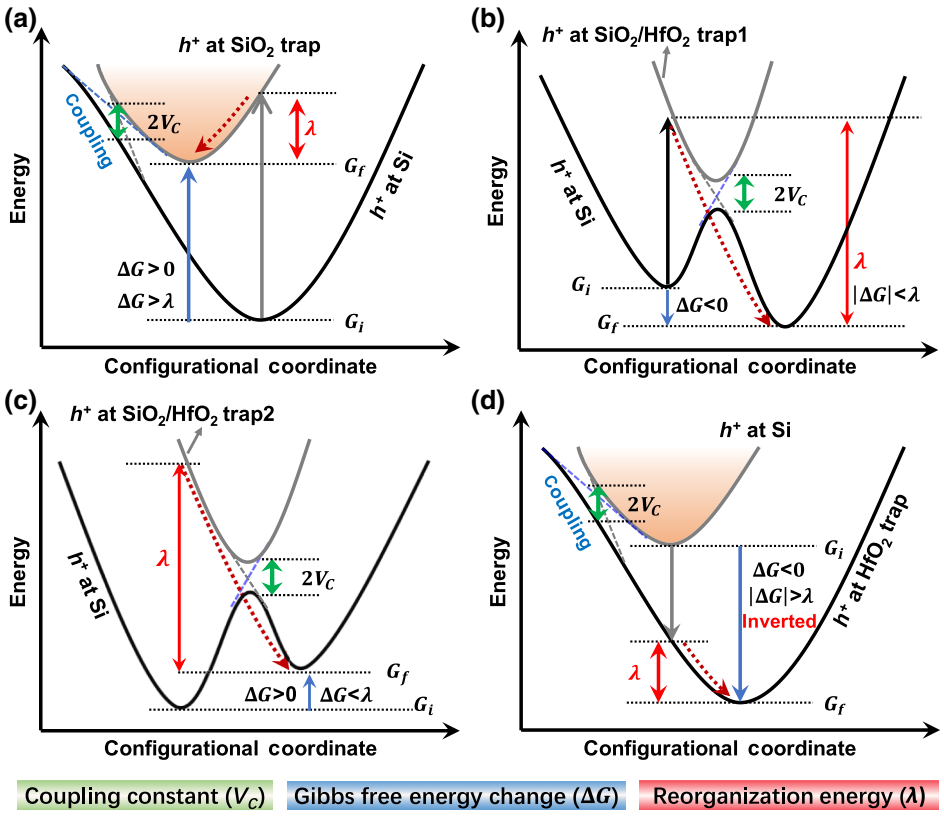

FIG. 2. Energy diagrams in configuration space for hole trapping from Si to the oxygen vacancy trap in (a) SiO_2, (b) SiO_2/HfO_2 interface trap1, (c) SiO_2/HfO_2 interface trap2, and (d) HfO_2. The three key factors in Marcus theory are marked in each case. The two SiO_2/HfO_2 interface defects are marked and distinguished in Fig. 3.

system becomes

$$G_f = E_0 - E_{\text{defect}} - \lambda_{\text{defect}}, \tag{3}$$

where λ_{defect} is the reorganization energy caused by the structural relaxation of atoms around the defect.

Since the wave function of the E_{VBM} is very delocalized, structural relaxation caused by hole occupation in the E_{VBM} should be negligible, and thus, λ_{Si} is treated as zero. On the contrary, λ_{defect} is usually large due to the localized nature of defect states and strong electron-phonon coupling. Therefore, the Gibbs energy change of the hole-trapping process can be written as

$$\Delta G = G_f - G_i = E_{\text{VBM}} - E_{\text{defect}} - \lambda_{\text{defect}}. \tag{4}$$

The overall λ can also be taken as λ_{defect}, if we ignore λ_{Si}. With the definitions of ΔG, λ, and V_C known, the difficulty lies in how to calculate them accurately in a Si/SiO_2/high-κ system. First, we should build a structure with an explicit interface, so that the effect of such multiple interfaces can be studied thoroughly. Second, we must conduct high-accuracy DFT calculations on the whole interface system to obtain the correct band gap and band alignment. This is very important for charge-trapping simulations because the charge-trapping rate depends exponentially on the energy barrier between the silicon band and defect levels. For this purpose, we use the Heyd-Scuseria-Ernzerhof (HSE) hybrid exchange-correlation functional instead of local-density approximations (LDA) or generalized gradient approximations (GGA) because the last two usually underestimate the band gap [31]. Third, a more direct method should be used to obtain the coupling constant accurately, under the realistic atomistic environment, especially with atomistic interfaces taken into consideration. Finally, a hole should be precisely inserted (trapped) to the targeted defect level to obtain the correct reorganization energy. With all of these key quantities obtained, the state-to-state hole-trapping rate can be calculated using Eq. (1).

B. Atomistic models

We first construct two $Si/SiO_2/HfO_2$ interface models, as shown in Figs. 3(a) and 3(b), which differ from each other in the thickness of the SiO_2 interlayer. The phases of SiO_2 and HfO_2 are β-cristobalite and monoclinic, respectively, and the orientation of the structure is (001). The side length of the unit cell is set as 10.86×10.86 Å^2, which is the size of the relaxed Si part. The strain of the SiO_2 part with respect to the Si and HfO_2 parts is -6.69% and -2%, respectively. These settings are chosen and determined by carefully referencing previous works [21,32–34]. The effect of strain on defect formation energy can be found in several recent works [35,36]. The marked oxygen atoms in Fig. 3 are the oxygen vacancies that have been studied in this work. Each defect is denoted by a phrase,

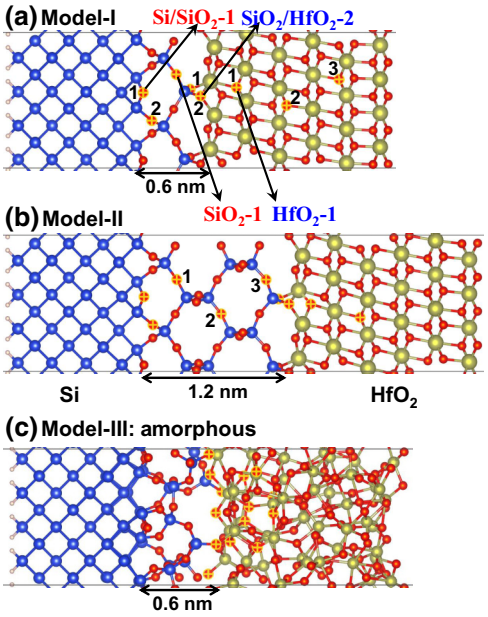

FIG. 3. (a) and (b) Two (001)-oriented $Si/SiO_2/HfO_2$ gate stack models with 0.6 and 1.2 nm interlayers, respectively. Oxygen vacancies at different locations, i.e., Si/SiO_2 interface, SiO_2 interlayer, SiO_2/HfO_2 interface, and HfO_2 high-κ layer, are numbered separately. (c) The $cSi/aSiO_2/aHfO_2$ stack used for the statistical study.

combining defect location with the defect order number. For example, Si/SiO_2-1 is the first defect at the Si/SiO_2 interface. To reveal the important role of dangling bonds at the Si/SiO_2 interface, and in seeking for a solution to weaken the trapping capability of the dominant hole traps, we also attempt to passivate all oxygen vacancies by H and F atoms. Lastly, we create an amorphous $Si/SiO_2/HfO_2$ structure ($cSi/aSiO_2/aHfO_2$) by MD simulations through the melt-quench process, to study the statistical property of charge trapping in a disordered system. Six interfacial oxygen vacancies and eight HfO_2 oxygen vacancies are sampled and labeled in Fig. 3(c). We note that a metal gate could affect the work function at the metal/HfO2 interface [37], but it will not change the physical picture of charge trapping from Si to the trap states in SiO_2 and HfO_2 layers.

The MD simulation is carried out by the QuantumATK 2018.6 program [38,39] (ATK), and the force field is from Ref. [40]. A Langevin thermostat is adopted in the whole melt-quench process, and a timestep of 1 fs is used. The melt process begins with an enlarged supercell, as reported in previous studies [41,42], to facilitate bond breaking, and it lasts for 50 ns under a temperature of 5000 K. After that, the supercell is shrunk back and melted for another 50 ns under 5000 K. Finally, the system is cooled linearly from 5000 to 300 K within 500 ns, i.e., a cooling rate of 9.4 K/s, to get the final structure. One difficulty is that SiO_2 and HfO_2 will mix with each other, if we start the melting process with the whole crystalline interface structure. To avoid

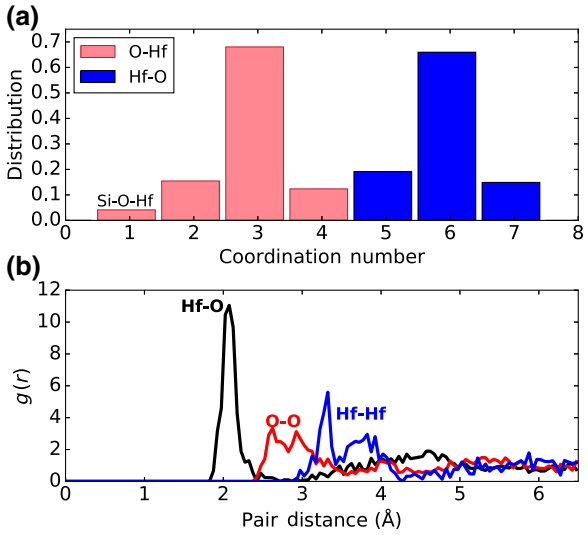

FIG. 4. The coordination number (a) and radial distribution function (b) of the amorphous HfO_2 part.

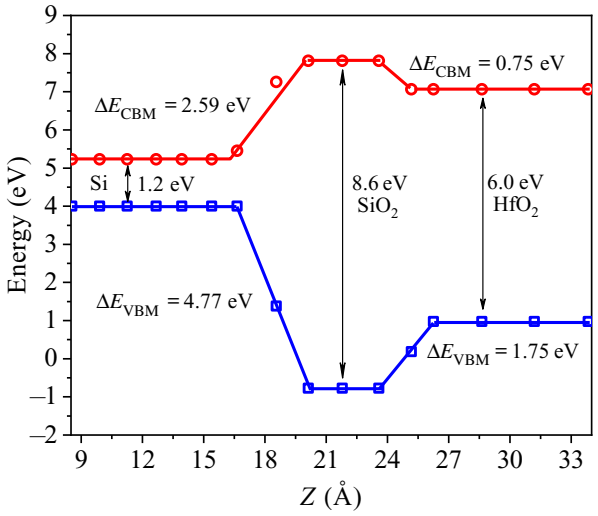

FIG. 5. Band alignment of the $Si/SiO_2/HfO_2$ system (model-II) calculated by density-functional theory with a hybrid functional (HSE). ΔE_{CBM} and ΔE_{VBM} indicate the conduction and valence band offsets, respectively.

that, we need to begin with a crystalline Si/SiO_2 stack and get crystalline-Si/amorphous-SiO_2 first, and then put crystalline HfO_2 into the supercell and melt HfO_2, while keeping the SiO_2 part fixed.

The quality of amorphous HfO_2 is confirmed by checking the coordination of each atom and the radial distribution function (RDF) of them, as shown in Fig. 4. In agreement with previous theoretical and experimental works [43–45], the coordination number of Hf atom is dominated by six, while accompanied by a few five and seven, and that of the O atom is dominated by three, with a few two and four. The one-coordinated O atom is that at the SiO_2/HfO_2 interface, bridging the Si and Hf atoms. Also, consistent with previous works [46–48], the Hf–O RDF peaks at about 2.1 Å, while those of O–O and Hf–Hf are distributed around 2.8 and 3.5 Å.

C. Density-functional theory simulations

DFT simulations are carried out by the plane-wave package PWmat with graphics processing unit (GPU) acceleration [49,50]. The GGA Perdew-Burke-Ernzerhof (PBE) functional is used for structural relaxation with a convergence criterion of 0.01 eV/Å for the residual force. The hybrid HSE functional is used in all self-consistent field (SCF) calculations to obtain the correct band alignment and defect levels. The HSE functional is also used to calculate the reorganization energy to correct the PBE results. The SG15 norm-conserving pseudopotentials are adopted with an energy cutoff of 50 Ry. A single gamma point is sampled by considering the large superlattices and large number of atoms in each model. HSE parameters are set separately, with a mask function for different materials to obtain their correct band gaps simultaneously [51]. The parameter sets for bulk Si, SiO_2, and HfO_2 are determined by reproducing their reported band gaps of 1.12, 8.5, and 5.8 eV, respectively. With these parameters, band alignment of the $Si/SiO_2/HfO_2$ interface structure is obtained (Fig. 5). It can be seen that the band gaps that agree well with experiment values are realized simultaneously. Besides, it is found that the interface transition regions are not atomically sharp. Therefore, the local atomic nature of interfaces must be considered in a realistic simulation of the multi-interface gate stacks.

The reorganization energy, λ, for each defect is obtained by inserting a hole into the defective system and then relaxing the system and recording the energy change. Since this relaxation is a local effect, we can calculate it based on pure bulk SiO_2 and HfO_2, or with the SO_2/HfO_2 interface system without Si. This has the advantage that the defect level will be inside the band gap, and thus, will not hybridize with the Si inner band states, which can make the charged defect atomic relaxation intractable. More specifically, we first relax the atomic structure with a defect in its neutral state (N electrons) and obtain an atomic structure R_0. Then, we remove an electron from the R_0 structure (N–1 electrons) and, without relaxation of the atomic positions, carry out an electronic structure self-consistent calculation to obtain the total energy, $E(R_0, N–1)$. The electron is, in fact, removed from the defect level because the defect level lies at the band gap and is the highest occupied level. After that, we relax the atomic structure with N–1 electrons to obtain its minimum energy, $E(R_1, N–1)$. The energy differences between these two atomic configurations (both with N–1 electrons) is the reorganization energy:

$$\lambda = E(R_0, N-1) - E(R_1, N-1). \tag{5}$$

Notably, since both energies have N–1 electron, they both have electrostatic image energies, and thus, there is no need for image interaction correction. The uncertainty caused by this electrostatic image interaction for the calculation of λ should thus be much smaller than that of typical defect-level calculations, where $E(N+1)$ and $E(N)$ are subtracted.

The Gibbs free energy change, ΔG, can be obtained straightforwardly, according to Eq. (4), once the band alignment, defect levels, and reorganization energy are known. The most difficult, but important, task is to calculate the coupling constant, V_C. In previous studies, V_C is often obtained by using the WKB approximation [16,17],

$$V_C = k_t \exp\left(-\frac{\sqrt{2m_t \Delta E}}{\hbar} d\right), \tag{6}$$

where ΔE is a tunneling barrier, m_t is the tunneling effective mass, and the parameter k_t can only be obtained by calibration with experiments. Such an approximation treats the coupling of two states as the tunneling of one state to the other, and it is not capable of taking into account the explicit atomic environment. Moreover, the WKB approximation has only been used in single-interface systems, such as Si/SiO_2, and its validity in multiple-interface systems is questionable (as the wave function can be bounced at the interface). Even in the single-interface Si/SiO_2 system, our previous work has shown that the WKB approximation can underestimate the coupling strength of two states [18].

In our more accurate approach, V_C will be obtained by direct DFT calculations. Considering a two-state system with coupling constant V_C that is subjected to an external field, we can write the Hamiltonian of the system by denoting the original energy difference of the two levels as $\Delta\epsilon_0$ and the field induced potential change as F:

$$H = \begin{pmatrix} -\Delta\varepsilon_0/2 + eF & V_C \\ V_C & \Delta\varepsilon_0/2 - eF \end{pmatrix}. \tag{7}$$

Diagonalizing this 2×2 Hamiltonian, we can obtain the eigenenergies of these two states:

$$\varepsilon_{\pm} = \pm\sqrt{V_C^2 + \left(\frac{\Delta\varepsilon_0}{2} - eF\right)^2}. \tag{8}$$

It can be seen that the two levels will get closer to each other under a certain field, but they will never cross each other due to their coupling. The minimum energy gap of the two levels is found to be exactly two times the coupling constant, V_C. Guided by this theory, we intentionally apply an electric field to the $Si/SiO_2/HfO_2$ structure, to drive the E_{VBM} and E_{defect} close to each other, until the anticrossing (avoid crossing) phenomenon occurs.

In summary, the theoretical simulation framework contains two steps. First, carrying out DFT calculations to obtain the parameters needed by Marcus theory, and then inputting them into the Marcus charge-transfer formula to get the exact trapping rate. The workflow of this scheme is shown in Fig. 6. With this framework, we can now investigate the charge-trapping process in any multilayered structures.

III. RESULTS AND DISCUSSION

From Eq. (1), it can be seen that hole trapping from the E_{VBM} to a defect in the dielectric layer is more likely to

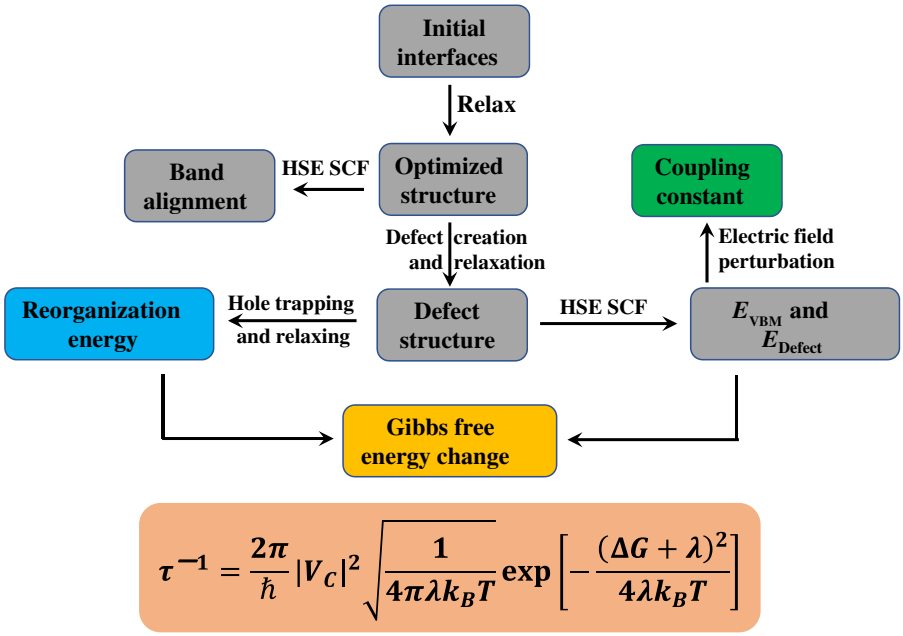

FIG. 6. Flowchart of the theoretical simulation framework, including sophisticated DFT calculations and the Marcus charge-trapping theory.

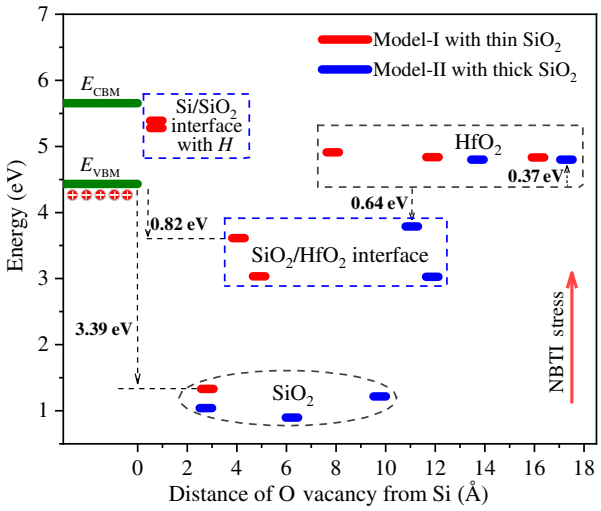

FIG. 7. The defect-level alignments of multiple-source V_O centers with respect to the Si band edge. The V_O defect state at the Si/SiO_2 interface is not local, unless a H atom is induced. NBTI, negative bias temperature instability.

happen when the defect level is close to the E_{VBM} and when the coupling constant between the two states is large. However, as we will see in Sec. III A and III B, these two conditions are usually opposing each other, and hence, they are difficult to satisfy at the same time. The balance between these two factors dominates hole or charge trapping in the $Si/SiO_2/HfO_2$ system.

A. Defect level and Si band edge alignment

Figure 7 summarizes the defect-level alignment of multiple-source V_O centers with respect to the Si band edge. Obviously, the V_O defects at different positions produce distinct defect levels. First, we find that the V_O defects at the Si/SiO_2 interface will not induce any local defect states near the E_{VBM}, unless a hydrogen atom is introduced. Second, the V_O defects inside the SiO_2 interlayer are deeply below the E_{VBM}, indicating that they are rarely able to trap holes. Third, those at the SiO_2/HfO_2 interface also lie below the E_{VBM}, but are much closer to the E_{VBM} in energy, which means that they are more advantageous in hole trapping. Last, the V_O defects at the HfO_2 layer lie very slightly above the E_{VBM}, making them the most energetically favorable hole traps. Nevertheless, it is worth mentioning that all the defect levels will be raised up by NBTI stresses for a p-type FET where hole trapping takes place. So, the hole-trapping capability will change according to the gate electric-field amplitude.

B. E_{VBM}-E_{defect} coupling

Figure 8 depicts the coupling and anticrossing energy curves between E_{VBM} and two V_O defects. The two V_O defects vary in location and their distance from Si, and thus, couple with different strengths with the E_{VBM}. For the first defect at the SiO_2 interlayer, as shown in Fig. 8(a), it can be seen that the wave function of E_{defect} is significantly localized at the oxygen vacancy before strong coupling, and the E_{VBM} is much more delocalized at the Si atoms. Upon further approach of the two energy levels, their wave functions begin to overlap with each other, and they localize at the same position when they couple the most. After that, these two states separate and the characters of the E_{VBM} and E_{defect} state will be switched. From the minimum gap of these two curves, one can obtain the $2V_C$ amplitude. The second defect, shown in Fig. 8(b), is a defect at the HfO_2 layer. The coupling process is nearly the same as that in Fig. 8(a), but the coupling constant is much smaller in value. This is because the V_O defect at HfO_2 is farther away from silicon and there is an interface in between.

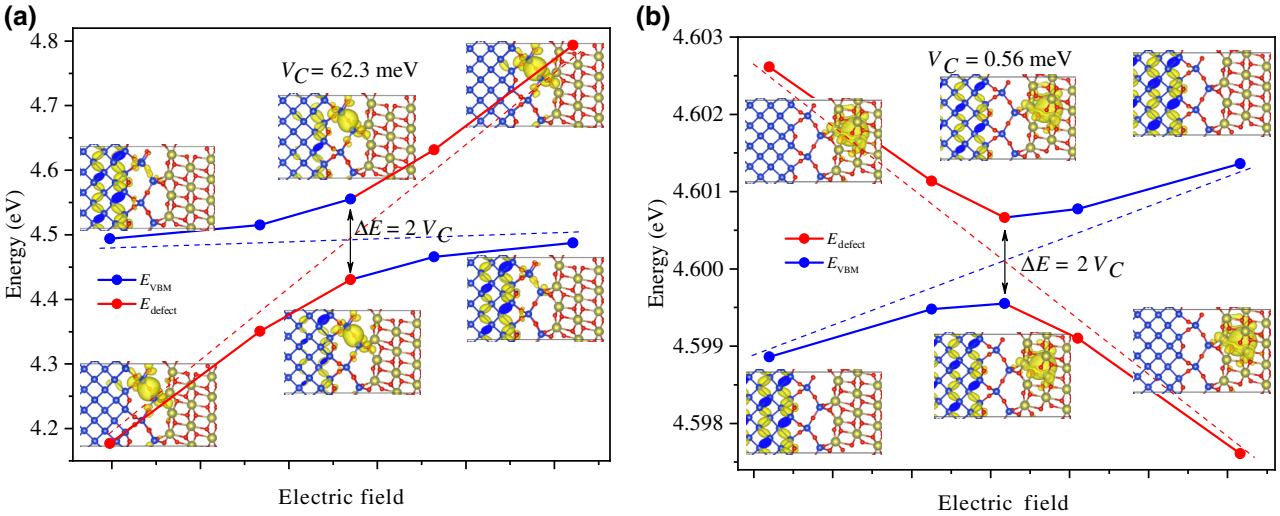

FIG. 8. The coupling process of the E_{VBM} with V_O defect in (a) SiO_2 interlayer and (b) HfO_2 high-κ layer.

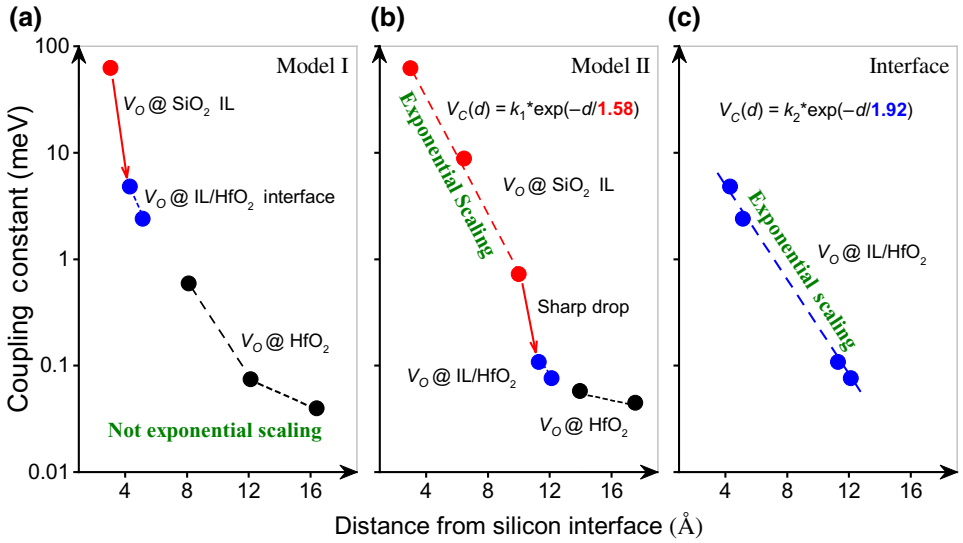

FIG. 9. Decay of the coupling constant with the distance of V_O defect from the Si substrate.

The coupling constants of the E_{VBM} with all other V_O defect levels are obtained by the same procedure and are shown in Fig. 9. Obviously, the coupling constants decrease monotonically with the distance of the defects from the Si substrate. However, it is also evident that the decay behavior of V_C can be divided into three types, according to the V_O defect locations. First, it can be seen from Fig. 9(b) that the V_C decay at the SiO_2 interlayer follows a good exponential trend with a decay length of 1.58 Å. However, it will experience a sharp drop when encountering the SiO_2/HfO_2 interface. If we put the interface defects of the two models together, as is seen in Fig. 9(c), we can also see an exponential trend but with a different scaling length (1.92 Å). More importantly, we find from Fig. 9(a) that the V_C decay in the high-κ HfO_2 layer does not follow a simple exponential law. These results mean that the coupling constant decay in a single interface system, e.g., Si/SiO_2, can be qualitatively described by a simple exponential function, such as the WKB approximation, but the V_C decay in multi-interface high-κ stacks, e.g., $Si/SiO_2/HfO_2$, is more complicated, and it cannot be described by a simple exponential function.

C. Reorganization energy

The effect of electron-phonon interaction is included in the reorganization energy, i.e., the energy change caused by structural relaxation after charge trapping. Figure 10 illustrates the reorganization process for three typical V_O defect locations. There is a common feature that all atoms around the vacancy defect will depart more from each other after hole trapping. However, the reorganization energy value differs because of the different local environment. By using the PBE functional, it is found that the V_O defect at the SiO_2 interlayer has a reorganization energy of 0.31 eV, while the SiO_2/HfO_2 interface and HfO_2 V_O defects have values around 1 eV.

Although these DFT results are expected to be relatively correct, we always question whether the choice of functional (e.g., PBE and HSE) will affect the calculation of the reorganization energy, especially because the level of charge localization and polaronic energy depend on the functional used, and sometimes PBE gives delocalized solutions when the physically correct picture is that of a localized charge.

To answer this question, we build two smaller models containing 96 atoms, of which one is crystalline HfO_2 and the other one is SiO_2, so that structural relaxation by the HSE functional is available. Then we sample two V_O defects (3-coordinated and 4-coordinated) in HfO_2 and one

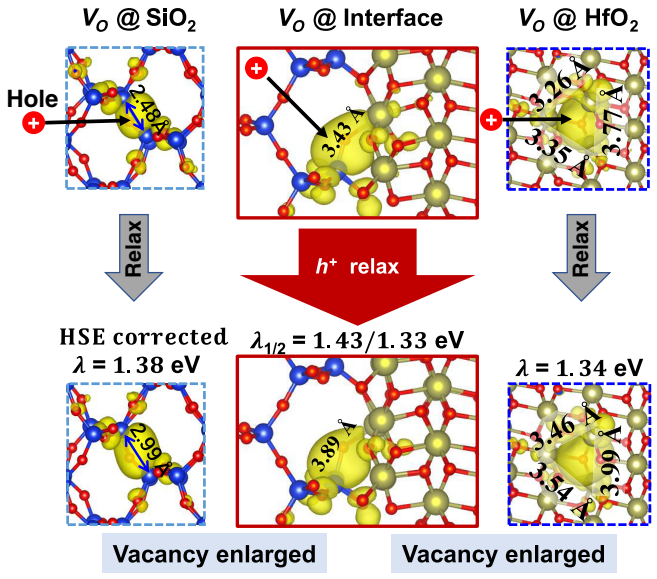

FIG. 10. The structural relaxation after hole trapping and the reorganization energy for V_O defects at (a) SiO_2, (b) SiO_2/HfO_2 interface, and (c) HfO_2. All the values are corrected by HSE functional calculations.

V_O defect in SiO_2 to calculate the reorganization energy with the PBE and HSE functionals, respectively. See Figs. S1–S3 within the Supplemental Material for the models and detailed comparison results [52]. It is found that the HSE functional generally produces a larger reorganization energy than that of the PBE functional. For both kinds of V_O defects in HfO_2, the HSE result is larger than that of the PBE result by a factor of about 1.4. For the V_O defect in SiO_2, when we calculate the electronic structure using the PBE functional under neutral-defect atomic positions, but occupying it with one hole (and thus, making it a "+" charged state), due to state hybridization with the VBM state, after SCF steps, the hole does not stay in the localized defect state that shown in Fig. 10(a), but instead it occupies a delocalized state, which changes the physical meaning for the reorganization energy. To correct this problem, we force the hole in the original localized defect state (from the neutral-state SCF calculation) into a constrained DFT scheme, and keep the hole state unchanged during SCF iterations. The atomic relaxed "+" charged state does not have this problem, and thus, can be calculated in a more conventional way. The calculated PBE reorganization energy is 0.99 eV, which is also about 1.4 times smaller than that of the corresponding HSE result (1.38 eV). We also test the effect of the functional on the H-passivated V_O defects and find a slightly different ratio between the PBE and HSE results. See Figs. S4, S5 within the Supplemental Material for the simulation results [52].

In summary, the PBE functional always produces a smaller reorganization energy than that of the HSE functional, probably due to larger wave function delocalization, but the PBE results can be approximately corrected by multiplying an amplification factor that depends on the defect type. For the V_O defect in SiO_2 and HfO_2, the correction factor is 1.4, while for a single-H passivated defect the correction factor is 1.1 and for a double-H passivated defect the correction factor is 1.3.

D. Hole-trapping rates

With all decisive parameters in hand, the hole-trapping rates can be calculated by using Eq. (1). The trapping rates for the V_O defects at the SiO_2 interlayer are too small to be shown here, so there are only data for V_O defects at the SiO_2/HfO_2 interface and the HfO_2 layer in Fig. 11. First, we discuss the case when the gate voltage is zero. It can be seen that the trapping rates to the HfO_2 layer V_O defects are very high, but not always the highest, even though these V_O defects are closest to the E_{VBM} in energy. This is because they are very far away from the Si substrate, and thus, their coupling with the E_{VBM} is very weak. On the contrary, the V_O defects at the SiO_2/HfO_2 interface couple much more strongly with the E_{VBM} due to a smaller distance to Si, so their hole-trapping capability can be stronger, even though their energy barrier with the E_{VBM} is less favorable for hole trapping. These results manifest well in the balance between coupling constant and energy barrier in controlling the charge-trapping rate. Overall, the energy barrier between the E_{VBM} and E_{defect} is more dominant because it appears at the exponential component in Eq. (1).

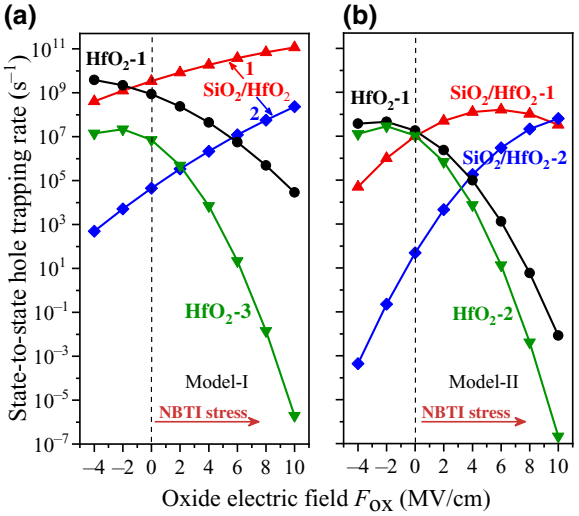

FIG. 11. The F_{OX}-dependent hole-trapping rate for different V_O defects in the case of model-I and model-II.

In a MOSFET, hole trapping is always dependent on the electric field. The oxide electric field will change the alignment of the defect level with respect to the E_{VBM} and thus. also change the energy barrier.

$$\Delta G = E_{VBM} - (E_{defect} + F_{OX}d) - \lambda_{defect}. \qquad (9)$$

where F_{OX} is the electric field induced by a negative gate voltage and d is the distance between the Si substrate and the V_O defect. Taking this realignment into account, the F_{OX}-dependent hole-trapping rates are calculated and also shown in Fig. 11. Since all defect levels will be raised up by the NBTI stresses, the interfacial V_O defects will get closer to the E_{VBM} and become more energetically favorable for hole trapping. As a result, their trapping capability will become stronger. On the contrary, because the V_O defects at HfO_2 are already higher in energy than that of the E_{VBM} at zero electric field, the NBTI stress will further drag the energy level away from that of the E_{VBM}, which eventually enters the Marcus inverted region, so their trapping capability will be decreased [53]. Nevertheless, the V_O defects in the HfO_2 layer will always stay effective because the electric field in the high-κ layer is usually very weak.

E. Complicated effects of H and F passivation

The effects of H and F passivation on defect charge trapping are very complex and interesting. On one hand, it is widely known that proper passivation is able to reduce

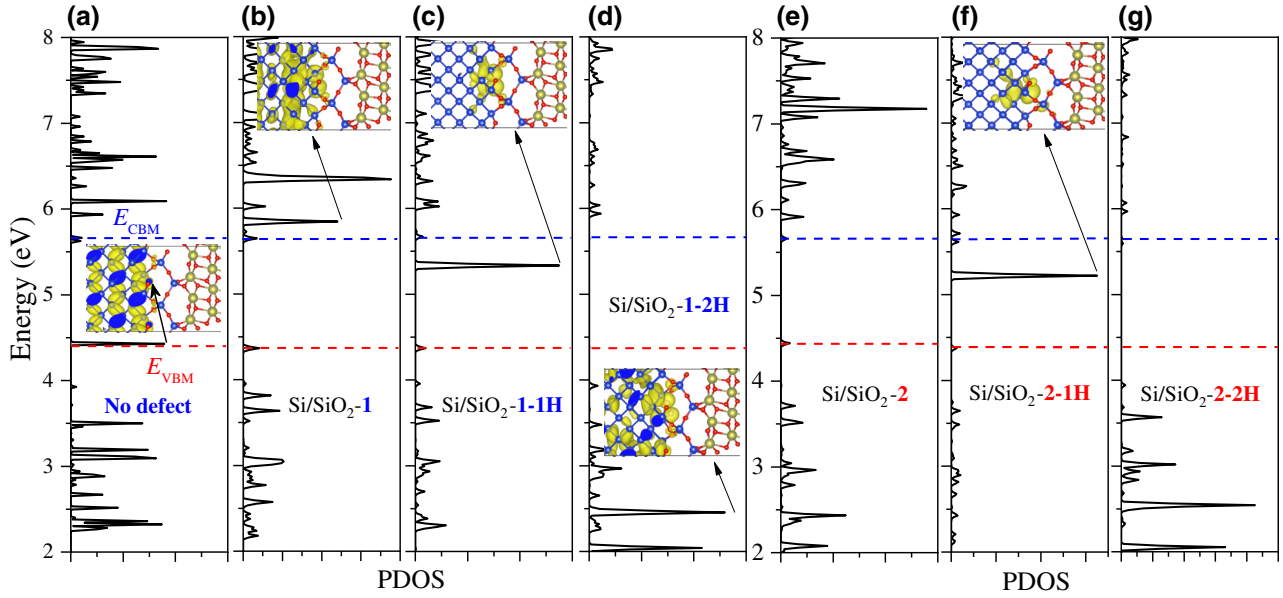

FIG. 12. PDOS and wave functions of oxygen vacancies at the Si/SiO_2 interface. (a) No vacancy, (b) first-V_O type with no passivation, (c) first-V_O type with single-H passivation, (d) first-V_O type with double-H passivation, and (e)–(g) second-V_O type. CBM, conduction band minimum; VBM, valence band maximum.

the defect state density to relieve the charge-trapping phenomenon [54–56]. On the other hand, it is also found that the forming and breaking of the Si–H bond at the Si/SiO_2 interface play important roles in charge transfer and BTI [57,58]. Moreover, F passivation is reported to be different from that of H passivation in relieving charge trapping in high-κ MOSFETs [59–61]. These phenomena naturally give rise to many questions, such as why is H passivation not as good as that of F in relieving charge trapping? Why are H atoms important for charge trapping at the Si/SiO_2 interface? In addition, is the effect of passivation the same for defects that are located at different parts of multilayer high-κ gate stacks? We use our theoretical simulations to help answer these questions.

First, we look at the effect of H atoms on the V_O defects at the Si/SiO_2 interface. It can be seen from the models in Fig. 3 that there are two kinds of V_O defect at the Si/SiO_2 interface, according to their local bonding environments. The first Si/SiO_2 V_O defect lies between two Si atoms that belong to bulk silicon, and the second V_O defect lies between bulk Si and SiO_2. The energy levels of these two defects before and after H passivation are all obtained by checking the partial density of states (PDOS) of the atoms around the defect, and are shown in Fig. 12. As mentioned in Sec. III A, there are no strong local defect states inside or near the band gap when the defect is not passivated, as observed in Fig. 12(b). Two strong PDOS peaks slightly above the Si CBM might indicate defect states. However, a closer investigation of the actual states near those energies shows that not only do they have a strong charge at the defect site, but they also have a charge density at Si. It is possible that the defect state is hybridized strongly with the bulk Si state. The case of V_O defects with double-H passivation is also similar, as shown in Fig. 12(d). For double-H passivation, the PDOS peaks are far below the VBM, which indicates that passivation has pushed them all the way from the conduction band into the valence band. In contrast, for the V_O with only one H, the defect state has been pushed down, from above the CBM into the band gap, but not all the way into the VB, as shown in the PDOS of Fig. 12(c). As a result, the corresponding wave function is very localized. Such a phenomenon is also observed in the second Si/SiO_2 interface defect, as shown in Figs. 12(e)–12(g). All of these results show a complicated story of H passivation at the Si/SiO_2 interface.

Following the framework shown in Fig. 6, the hole-trapping rates from the E_{VBM} to these single-H passivated Si/SiO_2 interface defects are obtained and shown in Fig. 13(a). In comparison with the main hole-trapping centers shown in Fig. 11, we find that these Si/SiO_2 interface defects are weaker at hole trapping under NBTI stresses. The reason is multifold. First, the energy barrier of H-passivated Si/SiO_2 interface defects is much larger than those at the HfO_2 layer, as observed in Fig. 7. Second, and more importantly, the reorganization energy of H-passivated Si/SiO_2 interface defects is found to be very small, as shown in Figs. 13(b) and 13(c). These energies are only 1/3 to 1/2 of those of unpassivated V_O at the SiO_2/HfO_2 interface and HfO_2 layer. Moreover, their trapping capability is further weakened by the NBTI stresses because the defect levels lie above that of the E_{VBM},

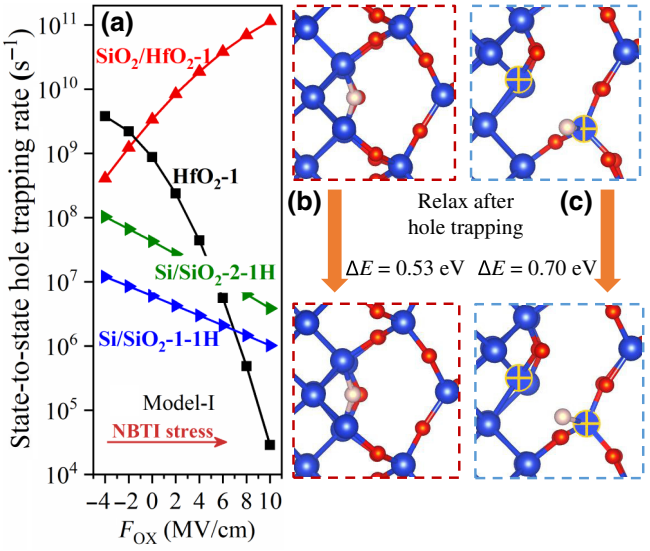

FIG. 13. (a) Comparison of hole-trapping rate from the E_{VBM} to V_O defects at the SiO_2/HfO_2 interface, HfO_2, and H-passivated Si/SiO_2 interface. (b) and (c) The reorganization of two kinds of V_O defects at the Si/SiO_2 interface, both with single-H passivation.

which will be raised up and further increase the energy barrier.

In contrast to the Si/SiO_2 interfacial V_O defects, the V_O defects in other locations will directly induce a very localized defect state near the E_{VBM}, as shown in Figs. 7 and 10. Therefore, the effect of passivation on these locations is supposed to be very different from that on the Si/SiO_2 interface. With the purpose of distinguishing the effects of H and F passivation, we carry out a study on H and F passivation on V_O defects in all locations.

Figure 14(a) shows the energy alignment of the Si band edge and the H-passivated V_O defects at different locations. Both single-H passivation and double-H passivation are studied. Compared with the defect levels without passivation (denoted by gray star lines), it can be seen that single-H passivation will push all V_O defect levels upwards, while double-H passivation will pull them down. Besides, the localized defect state will disappear when the V_O defects at SiO_2 are passivated by double-H atoms. Nevertheless, neither single-H passivation nor double-H passivation are able to completely eliminate the hole-trapping problem. For single-H passivation, the SiO_2 V_O defect and the second SiO_2/HfO_2 interface V_O defect are close to the E_{VBM}, and thus, are effective traps. Double-H passivation is better at relieving hole trapping, but the first SiO_2/HfO_2 interface V_O defect and the HfO_2 V_O defect are still not far from the E_{VBM}, and thus, are likely to be effective traps. We next calculate the coupling constants and reorganization energy of each defect, which are shown in Fig. 14(b). The resulting hole-trapping rates under different magnitudes of electric field are shown in Fig. 14(c). Under negative gate voltages, it can be seen from Fig. 14(c) that V_O-1H at the SiO_2 layer and the V_O-2H at the SiO_2/HfO_2 interface will both be active hole-trapping centers.

The effect of F passivation is very different from that of H passivation. It can be seen from Figs. 15(a)–15(c) that a single F atom can perfectly replace the O atom, regardless of the location at the SiO_2 layer, the SiO_2/HfO_2 interface, or the HfO_2 layer. This is a bit surprising, since one might think a single F^- anion cannot replace an O^{2-} anion. Since there is no dangling bond with F passivation, there is also no obvious defect energy near the Si band edge, as observed in Fig. 15(d). The defect levels induced by a single-F passivation are far from that of the Si band edge, and thus, will not be able to trap holes, according to Eq. (1). Double-F passivation presents several different features. First, the relaxed locations of F atoms are different with single-F passivation. Second, the two F atoms will induce two localized states that are close in energy, as observed in Fig. 15(e). The two states differ in the charge density distribution. Despite these differences, we can clearly see the common feature that no localized state close to the Si band edge will be induced by F passivation. Consequently, the hole-trapping problem can

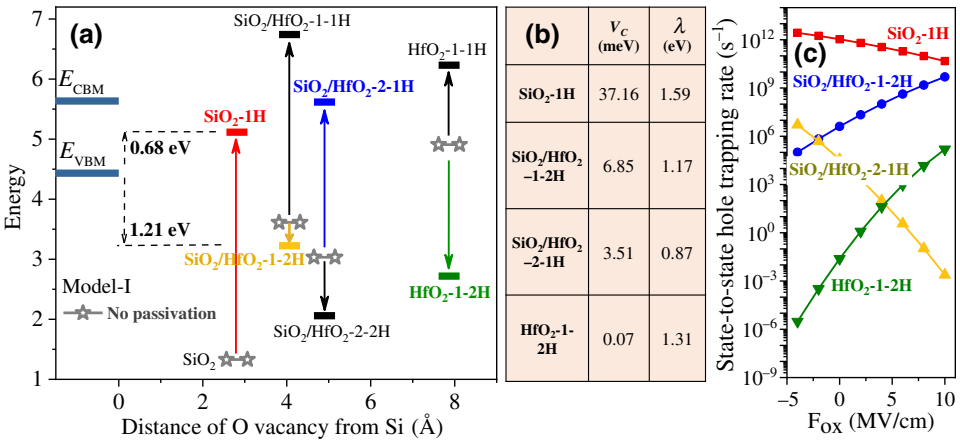

FIG. 14. (a) Energy alignment of V_O defects and the Si band edge before and after passivation, (b) the coupling constant and reorganization energy of each V_O defect, and (c) the electric-field-dependent hole-trapping rate from the E_{VBM} to four V_O defects that are most likely to be traps.

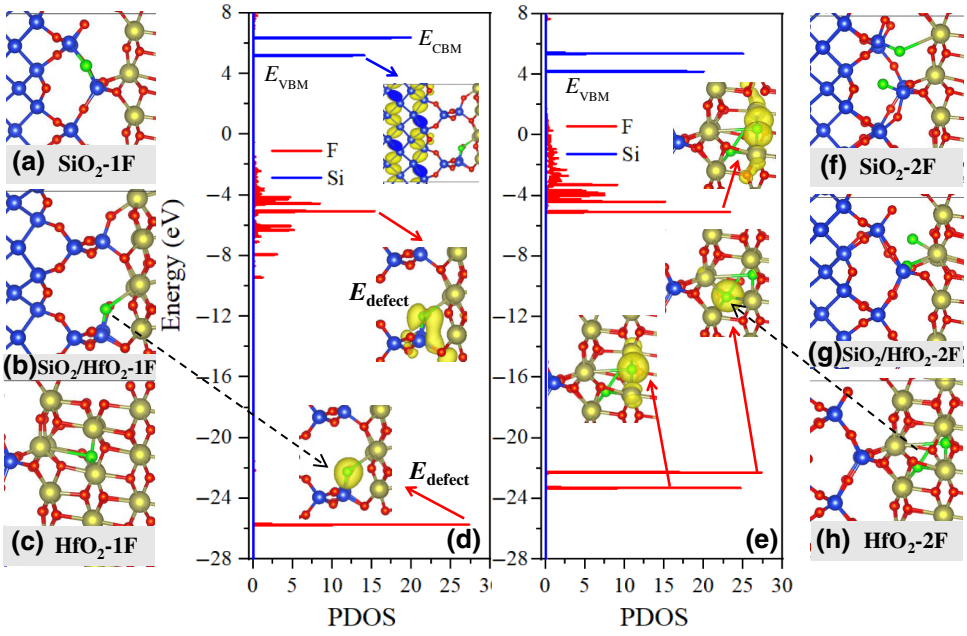

FIG. 15. Relaxed structures of F-passivated V_O defects and their PDOS. (a)–(c) Single-F passivation in SiO_2, SiO_2/HfO_2 interface, and HfO_2, respectively. (f)–(h) Double-F passivation in each position. (d) PDOS of the single-F atom at the SiO_2/HfO_2 interface. (e) PDOS of two F atoms at HfO_2.

be greatly relieved by F passivation, which is consistent with experimental observations [60].

F. Charge-trapping variation in amorphous $Si/SiO_2/HfO_2$ stacks

Although we note the distinct charge-trapping characteristics of defects at SiO_2, HfO_2, and their interfaces, it could still be of concern what happens in more complicated, but more realistic, amorphous $Si/SiO_2/HfO_2$ stacks. The local environment in amorphous stacks could be very different, even for the same kind of defects in the same material, not to mention at the interfaces. We note that the defect level of oxygen vacancies in an amorphous $Si/SiO_2/HfO_2$ stack has been reported before [62], but no further study on charge trapping or a statistical study on the defect level variation has been carried out. Therefore, we create the amorphous $Si/SiO_2/HfO_2$ stack shown in Fig. 3(c) to reveal charge-trapping variation in a disordered system and to look for information that cannot be extracted from crystalline stacks. As marked in Fig. 3(c), we sample six interface V_O defects and eight HfO_2 bulk V_Os. We also create a puckered V_O defect in SiO_2, as shown in the inset of Fig. 16, which is proven to exist in amorphous silica [63,64]. Then we calculate their defect levels, coupling constant with E_{VBM}, reorganization energy, and finally the hole-trapping rates under different magnitudes of electric fields.

The defect level of each V_O sample is shown in Fig. 16. Compared with the results in crystalline stacks, the consistent phenomenon is obvious, i.e., the defect levels induced by SiO_2 V_O defects and SiO_2/HfO_2 interface V_O defects are all below that of the E_{VBM}, and those induced by HfO_2 V_O defects are mostly above that of the E_{VBM}. On the other hand, several new phenomena are also easily observed. First, the puckered V_O defect in SiO_2 is much closer to the E_{VBM}, compared with the common dimer ones in crystalline SiO_2. Second, there are several four-coordinated V_O defects in $aHfO_2$, the defect level of which is slightly below that of the E_{VBM} instead of inside the Si band gap. Third, the defect levels at each material exhibit strong variation, which is accessible considering the disordered local environment in amorphous structures.

The variation also shows itself in the coupling constants and reorganization energy of each defect in Fig. 17. For the coupling constants shown in Fig. 17(a), we can still see a decreasing trend with an increasing distance of the

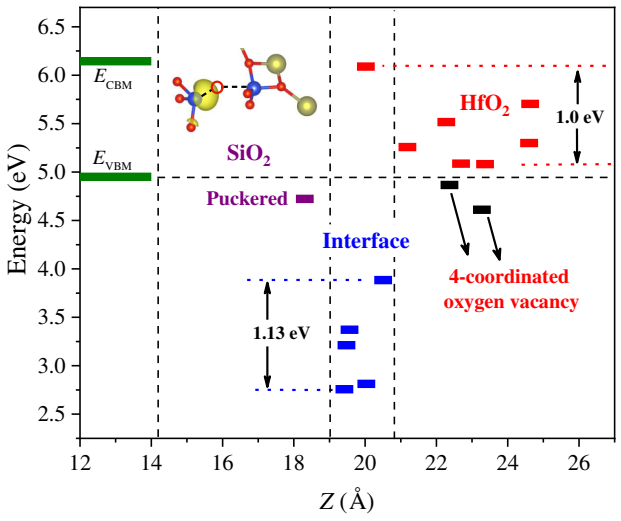

FIG. 16. Defect levels of the oxygen vacancies in $cSi/aSiO_2/aHfO_2$.

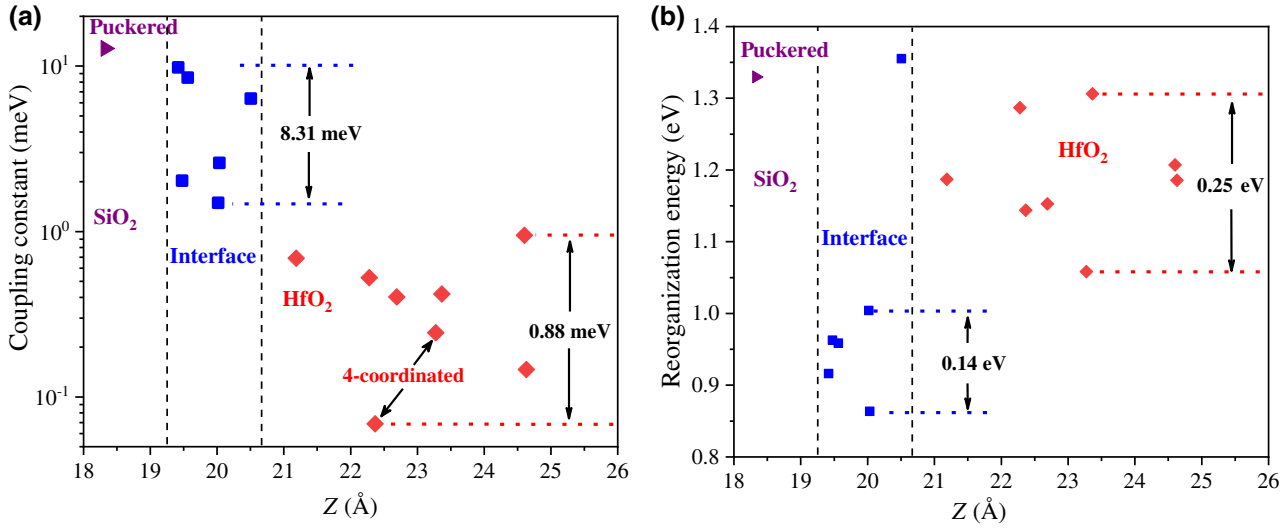

FIG. 17. (a) Coupling constant of each defect level with the E_{VBM}; (b) reorganization of each defect after hole trapping. All reorganization data are corrected by HSE functional calculations.

defect from Si, which is consistent with the case in the crystalline stack, but the trend is not strictly followed by every point. For the reorganization energy, the fluctuation is also obvious, even though the magnitude is less than one order.

Finally, we calculate the hole-trapping rate of each defect in the $\mathrm{cSi/aSiO_2/aHfO_2}$ stack, and their dependence on external electric field. Obviously, there are four kinds of defects in Fig. 18, i.e., the $\mathrm{SiO_2/HfO_2}$ interface V_Os, the hole-trapping capability of which increases monotonically with the electric field; the common $\mathrm{HfO_2}$ V_Os (2- and 3-coordinated). the hole-trapping rates of which decrease monotonically; the four-coordinated $\mathrm{HfO_2}$ V_Os. the trapping rates of which increase first and then decrease after a certain field strength; and the puckered $\mathrm{SiO_2}$ V_O defect, which is always a strong trapping center due to its closeness to Si in real space and its closeness to the E_{VBM} in energy. In comparison with the results in crystalline $\mathrm{Si/SiO_2/HfO_2}$ stacks, two new phenomena need to be pointed out. First, the strong hole-trapping rates of the puckered V_O defect in $\mathrm{SiO_2}$ overturns the previous conclusion that V_O defects in the $\mathrm{SiO_2}$ part are not effective hole-trapping centers, compared with those in $\mathrm{HfO_2}$ and the interface. Second, although some $\mathrm{SiO_2/HfO_2}$ interface defects are very effective in hole trapping, most of them are not as effective as the defects in $\mathrm{HfO_2}$. In other words, the amorphous $\mathrm{Si/SiO_2/HfO_2}$ stack shows us a more complete picture of hole trapping in high-κ gate stacks.

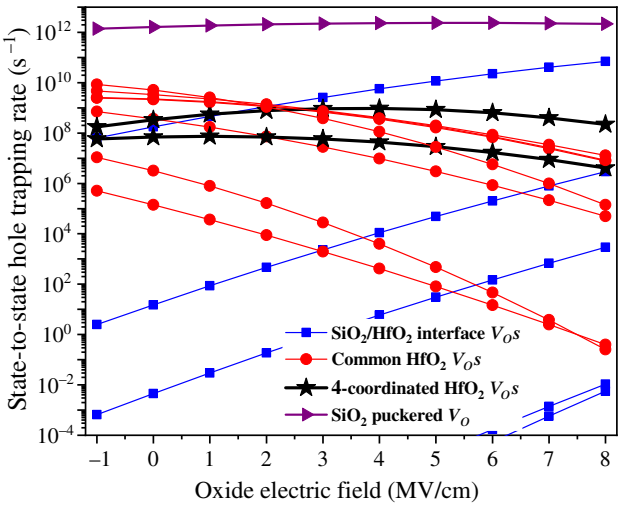

FIG. 18. Electric-field-dependent hole-trapping rate of each defect in the amorphous $\mathrm{Si/SiO_2/HfO_2}$ stack.

IV. CONCLUSIONS

Here, we propose an optimized theoretical simulation framework to study charge trapping across multiple interfaces. By applying this framework to crystalline and amorphous $\mathrm{Si/SiO_2/HfO_2}$ stacks, we can elucidate the hole-trapping mechanism for multiple trapping paths in the structure and identify the dominant hole-trapping centers by calculating the exact hole-trapping rates under different magnitudes of gate electric field. Results show that the dominant hole-trapping centers are neither located at a single material nor limit themselves to a single type. On the contrary, the strong hole-trapping center could be a puckered V_O defect or single-H passivated dimer V_O defect at $\mathrm{SiO_2}$, some V_O defects at the $\mathrm{SiO_2/HfO_2}$ interface, or most V_O defects inside the bulk $\mathrm{HfO_2}$. Moreover, we find that H passivation is not able to eliminate such a hole-trapping problem effectively due to the formation of some H-related defects, which are also effective trapping centers. On the

contrary, F passivation is more effective at eliminating defect states and should be further investigated. We hope that all of these conclusions are instructive in improving the performance of high-κ MOSFETs, and the simulation framework is helpful for studying the charge-trapping problems in other semiconductor devices.

ACKNOWLEDGMENTS

This work was supported by the National Natural Science Foundation of China (Grants No. 61927901, No. 11774338, and No. 11574304), the China Key Research and Development Program (Grant No. 2018YFA0306101), the Chinese Academy of Sciences-Peking University Pioneer Cooperation Team (CAS-PKU Pioneer Cooperation Team), the Youth Innovation Promotion Association CAS (Grant No. 2016109), and Grant No. 6J6011000. Y.Y.L. acknowledges support from the National Postdoctoral Program for Innovative Talents (Grant No. BX201700231) and the China Postdoctoral Science Foundation (Grant No. 2018M630194). L.W.W. is funded by the Joint Center for Artificial Photosynthesis, a DOE Energy Innovation Hub, supported through the Office of Science of the U.S. Department of Energy under Award No. DE-SC0004993.

[1] L. Larcher, A. Padovani, L. Vandelli, and P. Pavan, Charge transport in high-k stacks for charge-trapping memory applications: A modeling perspective, Microelectron. Eng. **88**, 1168 (2011).

[2] C. Zhao, C. Z. Zhao, S. Taylor, and P. R. Chalker, Review on Non-volatile memory with high-k dielectrics: Flash for generation beyond 32nm, Materials **7**, 5117 (2014).

[3] J. H. Stathis and S. Zafar, The negative bias temperature instability in MOS devices: A review, Microelectron. Reliab **46**, 270 (2006).

[4] T. Grasser, *et al.*, The paradigm shift in understanding the bias temperature instability: From reaction–diffusion to switching oxide traps, IEEE Trans. Electron Devices **58**, 3652 (2011).

[5] B. H. Lee, *et al.*, in *Proceedings of the IEEE International Electron Devices Meeting* (1999), pp. 133–136.

[6] E. P. Gusev, *et al.*, in *Proceedings of the IEEE International Electron Devices Meeting* (2001), pp. 451–454.

[7] J. Robertson, High dielectric constant oxides, Eur. Phys. J. Appl. Phys. **28**, 265 (2004).

[8] C.-L. Kuo and G. S. Hwang, Structure and Interconversion of Oxygen-Vacancy-Related Defects on Amorphous Silica, Phys. Rev. Lett. **97**, 066101 (2006).

[9] N. L. Anderson, R. P. Vedula, P. A. Schultz, R. M. Van Ginhoven, and A. Strachan, First-Principles Investigation of Low Energy E' Center Precursors in Amorphous Silica, Phys. Rev. Lett. **106**, 206402 (2011).

[10] A.-M. El-Sayed, M. B. Watkins, V. V. Afanas'ev, and A. L. Shluger, Nature of intrinsic and extrinsic electron trapping in SiO_2, Phys. Rev. B **89**, 125201 (2014).

[11] A.-M. El-Sayed, M. B. Watkins, T. Grasser, V. V. Afanas'ev, and A. L. Shluger, Hydrogen-Induced Rupture of Strained Si−O Bonds in Amorphous Silicon Dioxide, Phys. Rev. Lett. **114**, 115503 (2015).

[12] A.-M. El-Sayed, Y. Wimmer, W. Goes, T. Grasser, V. V. Afanas'ev, and A. L. Shluger, Theoretical models of hydrogen-induced defects in amorphous silicon dioxide, Phys. Rev. B **92**, 014107 (2015).

[13] E. Mehes and C. H. Patterson, Defects at the Si(001)/a-SiO_2 interface: Analysis of structures generated with classical force fields and density functional theory, Phys. Rev. Materials **1**, 044602 (2017).

[14] F. Cerbu, O. Madia, D. V. Andreev, S. Fadida, M. Eizenberg, L. Breuil, J. G. Lisoni, J. A. Kittl, J. Strand, A. L. Shluger, V. V. Afanas'ev, M. Houssa, and A. Stesmans, Intrinsic electron traps in atomic-layer deposited HfO_2 insulators, Appl. Phys. Lett. **108**, 222901 (2016).

[15] T. Grasser, B. Kaczer, W. Goes, Th. Aichinger, Ph. Hehenberger, and M. Nelhiebel, Understanding negative bias temperature instability in the context of hole trapping, Microelectron. Eng. **86**, 1876 (2009).

[16] T. Grasser, B. Kaczer, W. Goes, Th. Aichinger, Ph. Hehenberger, and M. Nelhiebel, A two stage model for negative bias temperature instability, Proc. Int. Rel. Phys. Symp, 33 (2009).

[17] W. Goes, Y. Wimmer, A.-M. El-Sayed, G. Rzepa, M. Jech, A. L. Shluger, and T. Grasser, Identification of oxide defects in semiconductor devices: A systematic approach linking DFT to rate equations and experimental evidence, Microelectron. Reliab. **87**, 286 (2018).

[18] Y.-Y. Liu, F. Zheng, X. Jiang, J.-W. Luo, S.-S. Li, and L.-W. Wang, Ab Initio Investigation of Charge Trapping Across the Crystalline-Si/Amorphous-SiO_2 Interface, Phys. Rev. Appl. **11**, 044058 (2019).

[19] A. S. Foster, F. L. Gejo, A. L. Shluger, and R. M. Nieminen, Vacancy and interstitial defects in hafnia, Phys. Rev. B **65**, 174117 (2002).

[20] K. Xiong, J. Robertson, M. C. Gibson, and S. J. Clark, Defect energy levels in HfO_2 high-dielectric-constant gate oxide, Appl. Phys. Lett. **87**, 183505 (2005).

[21] K. Takagi and T. Ono, First-principles study on leakage current caused by oxygen vacancies at $HfO_2/SiO_2/Si$ interface, Jpn. J. Appl. Phys. **57**, 066501 (2018).

[22] E. P. Gusev, C. D_Emic, S. Zafar, and A. Kumar, Charge trapping and detrapping in HfO_2 high-k gate stacks, Microelectron. Eng. **72**, 273 (2004).

[23] H. W. You and W. J. Cho, Charge trapping properties of the HfO_2 layer with various thicknesses for charge trap flash memory applications, Appl. Phys. Lett. **96**, 093506 (2010).

[24] J. Ji, Y. Qiu, S. Guo, R. Wang, P. Ren, P. Hao, and R. Huang, in *Proceedings of the IEEE International Electron Devices Meeting* (2014), pp. 542–545.

[25] K. Tarafder, Y. Surendranath, J. H. Olshansky, A. P. Alivisatos, and L.-W. Wang, Hole transfer dynamics from a CdSe/CdS quantum Rod to a tethered ferrocene derivative, J. Am. Chem. Soc. **136**, 5121 (2014).

[26] Y.-Y. Liu and X. Jiang, in *Proceedings of the IEEE International Electron Devices Meeting* (2018), pp. 922–925.

[27] R. A. Marcus, On the theory of oxidation-reduction reactions involving electron transfer. I, J. Chem. Phys. **24**, 966 (1956).

[28] R. A. Marcus, On the theory of electron-transfer reactions. VI. unified treatment for homogeneous and electrode reactions, J. Chem. Phys. **43**, 679 (1965).

[29] H. Wei, J.-W. Luo, S.-S. Li, and L.-W. Wang, Revealing the origin of fast electron transfer in TiO_2-based Dye-sensitized solar cells, J. Am. Chem. Soc. **138**, 8165 (2016).

[30] A. Massé, P. Friederich, F. Symalla, F. Liu, R. Nitsche, R. Coehoorn, W. Wenzel, and P. A. Bobbert, Ab initio charge-carrier mobility model for amorphous molecular semiconductors, Phys. Rev. B **93**, 195209 (2016).

[31] J. Heyd and G. E. Scuseria, Efficient hybrid density functional calculations in solids: Assessment of the heyd-scuseria-ernzerhof screened Coulomb hybrid functional, J. Chem. Phys. **121**, 1187 (2004).

[32] X. Wang, *et al.*, Band alignment of HfO_2 on SiO_2/Si structure, Appl. Phys. Lett. **100**, 122907 (2012).

[33] Y. Park, K.-j. Kong, H. Chang, and M. Shin, First-Principles studies of the electronic and dielectric properties of $Si/SiO_2/HfO_2$ interfaces, Jpn. J. Appl. Phys. **52**, 041803 (2013).

[34] E. Nadimi and M. Schreiber, The influence of lanthanum doping on the band alignment in $Si/SiO_2/HfO_2$ gate stack of nano-MOSFETs: A first principles investigation, Phys. Status Solidi B **254**, 1700147 (2017).

[35] U. Aschauer and N. A. Spaldin, Interplay between strain, defect charge state, and functionality in complex oxides, Appl. Phys. Lett. **109**, 031901 (2016).

[36] M. G. Sensoy, D. Vinichenko, W. Chen, C. M. Friend, and E. Kaxiras, Strain effects on the behavior of isolated and paired sulfur vacancy defects in monolayer MoS_2, Phys. Rev. B **95**, 014106 (2017).

[37] H. Zhu and R. Ramprasad, Effective work function of metals interfaced with dielectrics: A first-principles study of the Pt-HfO2 interface, Phys. Rev. B **83**, 081416(R) (2011).

[38] https://www.synopsys.com/silicon/quantumatk.html.

[39] J. Schneider, J. Hamaekers, S. T. Chill, S. Smidstrup, J. Bulin, R. Thesen, A. Blom, and K. Stokbro, ATK-ForceField: A new generation molecular dynamics software package, Modelling Simul. Mater. Sci. Eng. **25**, 085007 (2017).

[40] G. Broglia, G. Ori, L. Larcher, and M. Montorsi, Molecular dynamics simulation of amorphous HfO_2 for resistive RAM applications, Modell. Simul. Mater. Sci. Eng. **22**, 065006 (2014).

[41] E. A. Chagarov and A. C. Kummel, Ab initio molecular dynamics simulations of properties of a-Al_2O_3/vacuum and a-ZrO_2/vacuum vs a-Al_2O_3/Ge(100)(2×1) and a-ZrO_2/Ge(100)(2×1) interfaces, J. Chem. Phys. **130**, 124717 (2009).

[42] T.-J. Chen and C.-L. Kuo, First principles study of the structural, electronic, and dielectric properties of amorphous HfO_2, J. Appl. Phys. **110**, 064105 (2011).

[43] P. Broqvist, A. Alkauskas, and A. Pasquarello, Band alignments and defect levels in Si-HfO_2 gate stacks: Oxygen vacancy and Fermi-level pinning, Appl. Phys. Lett. **92**, 132911 (2008).

[44] G. H. Chen, Z. F. Hou, and X. G. Gong, Density functional calculations on atomic and electronic structures of amorphous HfO_2/Si(001) interface, Appl. Phys. Lett. **95**, 102905 (2009).

[45] L. C. Gallington, Y. Ghadar, L. B. Skinner, J. K. R. Weber, S. V. Ushakov, A. Navrotsky, A. Vazquez-Mayagoitia, J. C. Neuefeind, M. Stan, J. J. Low, and C. J. Benmore, The structure of liquid and amorphous hafnia, Materials **10**, 1290 (2017).

[46] C. Kaneta and T. Yamasaki, Oxygen-related defects in amorphous HfO_2 gate dielectrics, Microelectron. Eng. **84**, 2370 (2007).

[47] W. L. Scopel, A. J. R. da Silva, and A. Fazzio, Amorphous HfO_2 and $Hf_{1-x}Si_xO$ via a melt-and-quench scheme using ab initio molecular dynamics, Phys. Rev. B **77**, 172101 (2008).

[48] Y. Wang, F. Zahid, J. Wang, and H. Guo, Structure and dielectric properties of amorphous high-κ oxides: HfO_2, ZrO_2, and their alloys, Phys. Rev. B **85**, 224110 (2012).

[49] W. Jia, Z. Cao, L. Wang, J. Fu, X. Chi, W. Gao, and L.-W. Wang, The analysis of a plane wave pseudopotential density functional theory code on a GPU machine, Comput. Phys. Comm. **184**, 9 (2013).

[50] W. Jia, J. Fu, Z. Cao, L. Wang, X. Chi, W. Gao, and L.-W. Wang, Fast plane wave density functional theory molecular dynamics calculations on multi-GPU machines, J. Comput. Phys. **251**, 102 (2013).

[51] F. Zheng, H. H. Pham, and L.-W. Wang, Effects of the c-Si/a-SiO_2 interfacial atomic structure on its band alignment: An ab initio study, Phys. Chem. Chem. Phys. **19**, 32617 (2017).

[52] See the Supplemental Material at http://link.aps.org/supplemental/10.1103/PhysRevApplied.12.064012 for the influence of functional (PBE and HSE) on the reorganization energy.

[53] G. L. Closs, L. T. Calcaterra, N. J. Green, K. W. Penfield, and J. R. Miller, Distance, stereoelectronic effects, and the marcus inverted region in intramolecular electron transfer in organic radical anions, J. Phys. Chem. **90**, 3673 (1986).

[54] R. J. Carter, E. Cartier, A. Kerber, L. Pantisano, T. Schram, S. De Gendt, and M. Heyns, Passivation and interface state density of SiO_2/HfO_2-based/polycrystalline-Si gate stacks, Appl. Phys. Lett. **83**, 533 (2003).

[55] H. H. Tseng, P. J. Tobin, S. Kalpat, J. K. Schaeffer, M. E. Ramón, L. R. C. Fonseca, Z. X. Jiang, R. I. Hegde, D. H. Triyoso, and S. Semavedam, Defect passivation With fluorine and interface engineering for Hf-based high-k/metal gate stack device reliability and performance enhancement, IEEE Trans. Electron Devices **54**, 3267 (2007).

[56] C. H. Lee, T. Nishimura, T. Tabata, S. K. Wang, K. Nagashio, K. Kita, and A. Toriumi, in *Proceedings of the IEEE International Electron Devices Meeting* (2010), pp. 416–419.

[57] K. O. Jeppson and C. M. Svensson, Negative bias stress of MOS devices at high electric fields and degradation of MNOS devices, J. Appl. Phys. **48**, 2004 (1977).

[58] L. Tsetseris, X. J. Zhou, D. M. Fleetwood, R. D. Schrimpf, and S. T. Pantelides, Physical mechanisms of negative-bias temperature instability, Appl. Phys. Lett. **86**, 142103 (2005).

[59] T. B. Hook, E. Adler, F. Guarin, J. Lukaitis, N. Rovedo, and K. Schruefer, The effects of fluorine on parametrics and reliability in a 0.18-um 3.5/6.8 nm dual gate oxide CMOS technology, IEEE Trans. Electron Devices **48**, 1346 (2007).

[60] K. -i. Seo, R. Sreenivasan, P. C. McIntyre, and K. C. Saraswat, Improvement in high-k (HfO_2/SiO_2) reliability by incorporation of fluorine, IEEE Electron Device Lett. **27**, 821 (2006).

[61] Y. Liu, M. R. Halfmoon, C. A. Rittenhouse, and S. Wang, Passivation effects of fluorine and hydrogen at the SiC-SiO_2 interface, Appl. Phys. Lett. **97**, 242111 (2010).

[62] P. Broqvist, A. Alkauskas, J. Godet, and A. Pasquarello, First principles investigation of defect energy levels at semiconductor-oxide interfaces: Oxygen vacancies and hydrogen interstitials in the Si–SiO_2–HfO_2 stack, J. Appl. Phys. **105**, 061603 (2009).

[63] J. K. Rudra and W. B. Fowler, Oxygen vacancy and the E1' center in crystalline Si02, Phys. Rev. B **35**, 8223 (1987).

[64] S. Mukhopadhyay, P. V. Sushko, A. M. Stoneham, and A. L. Shluger, Modeling of the structure and properties of oxygen vacancies in amorphous silica, Phys. Rev. B **70**, 195203 (2004).